Original Research Article

Design and in silico screening of combinatorial library of new herbicidal analogs of Cycloalka[d]quinazoline-2,4dione−Benzoxazinones inhibiting Protoporphyrinogen IX Oxidase.

ABSTRACT:
We virtually design here an important new weedkiller Cycloalka[d]quinazoline-2,4dione−Benzoxazinones (CQB), inhibitors of Protoporphyrinogen IX Oxidase (PPO). Based on computer-assisted combinatorial chemistry techniques, docking, 3D-QSAR and pharmacophore models we first enumerate, focuse and *in silico* screen a virtual library of CQB analogs substituted at positions R_1, R_2 and R_3. By docking inhibitors into the target active site from the crystal structure (PDB ID: 1SEZ) of PPO in complex with a CQB ligand, 3D models of 29 PPO:CQBx complexes with known observed activity (K_i^{exp}) were prepared to establish a quantitative structure–activity (QSAR) model and linear correlation between relative Gibbs free energy (GFE) of receptor-ligand complex formation ($\Delta\Delta G_{com}$) and K_i^{exp}: $pK_i^{exp} = -0.1664\ \Delta\Delta G_{com} + 8.306$ (1); $R^2 = 0.94$. A 3D QSAR pharmacophore model (PH4) derived from the QSAR directed our effort to design novel CQB analogs. During the design, an initial virtual library of 118 CQB was focused down and PH4 screened to identify 28 promising novel analogs. Their K_i (K_i^{pre}) values were predicted by means of equation (1). The most active analog namely CQB22 display K_i^{pre} 22 times superior to that of the reported most active training set ligand 17i. Our survey proposes this compounds to the synthesis and to the assessment on herbicidal.

Keywords: CQB; PPO; docking; 3D-QSAR models; pharmacophore; in silico screening.

1. Introduction

Due to their detrimental impact on green plants and cultures survival bad herbs have drawn attention of research community in the design of herbicides addressing the United Nations sustainable development goal N°2 “Zero Hunger” [1]. Photosynthesis is the process by which green plants and some other organisms use sunlight to synthesize nutrients from carbon dioxide and water. Photosynthesis in plants generally involves the green pigment chlorophyll and generates oxygen as a product. In the plant’s life cycle, protoporphyrin IX is an important substrate involved in the biosynthesis of chlorophyll. It results from the oxidation of protoporphyrinogen IX [2,3] and its inhibition is lethal for the plants making it one of the most important herbicidal targets.

Recently Da Wei and al [4] suggest 36 compounds belonging to the class of the CQB with the best active namely 17i ***(Figure1)*** displaying a one digit nanomolar concentration range (K_i = 6.7nM). The interactions between PPO and 17i displayed in the 2D diagram (***Figure 2)*** has served as starting structural information for analogs docking, QSAR modeling. Others weedkiller [5,6,7], inhibitors of Protoporphyrinogen IX Oxidase (PPO), novel diphenyl ether derivatives have been proposed by Li-Xia Zhao *et al.* [8]. In this work we elaborate a 3D-QSAR pharmacophore model [9] derived from the QSAR model to serve as virtual library screening tool in the search of new herbicides.

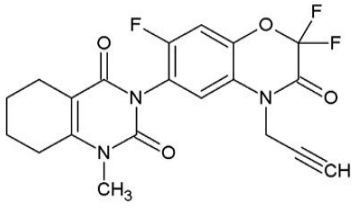

Figure1. *Chemical structure of herbicidal agents: Cycloalka[d]quinazoline-2,4dione−Benzoxazinones core (17i)*

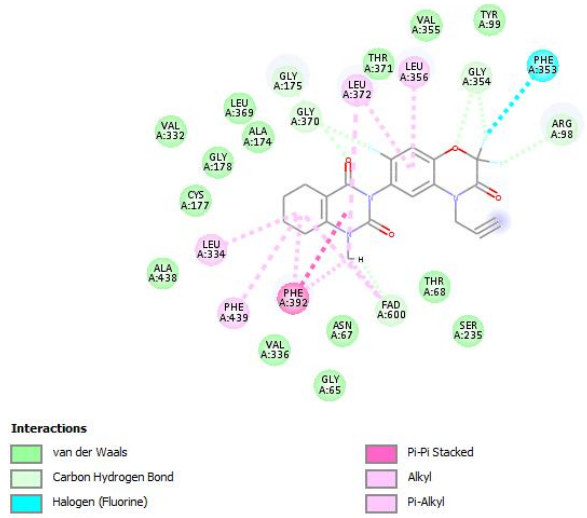

Figure2. *PPO-17i – ligand interactions at active site depicted in 2D for the most active CQB.*

2. MATERIALS AND METHODS

2.1. Training and validation sets

Chemical structures and biological activities (K_i^{exp}) of training and validation sets of CQB derivatives ligands of PPO used in this study were taken from literature [4].The potencies of these compounds cover a sufficiently broad range of half-maximal effective concentrations ($6.7 \leq K_i^{exp} \leq 2500$ nM) to allow construction of a QSAR model. The training set (TS) containing 29 CQBs ligands and the validation set (VS) including 7 CQBs were taken from the ref [4].

Table 1. *Training and validation set of PPO inhibitors for QSAR model.*

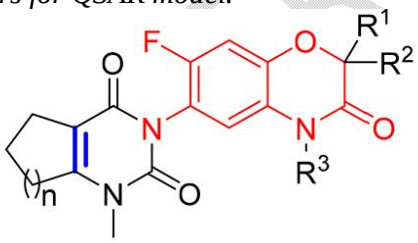

Training set	n	R^1	R^2	R^3	Ki(μM)
8a	1	H	H	$CH_2C_6H_4(4\text{-}OCH_3)$	210
8b	1	H	H	H	340
8c	1	H	H	CH_3	270
8d	1	H	H	CH_2CH_3	98
8e	1	H	H	$CH_2CH_2CH_3$	69
8g	1	H	H	$CH_2CH(CH_3)_2$	170
8h	1	H	H	$CH_2CH{=}CH_2$	20
8j	1	H	H	$CH_2C{\equiv}CSi(CH_3)_3$	2500
8k	1	H	H	$CH_2CO_2CH_2CH_3$	48
9a	2	H	H	$CH_2C_6H_4(4\text{-}OCH_3)$	200
9c	2	H	H	CH_3	160
9e	2	H	H	$CH_2CH_2CH_3$	44
9f	2	H	H	$CH_2CH_2CH_2CH_3$	46
9g	2	H	H	$CH_2CH(CH_3)_2$	100
9h	2	H	H	$CH_2CH{=}CH_2$	11
9j	2	H	H	$CH_2C{\equiv}CSi(CH_3)_3$	260
9k	2	H	H	$CH_2CO_2CH_2CH_3$	370
9l	2	H	H	CH_2CN	110
17a	2	F	F	$CH_2C_6H_4(4\text{-}OCH_3)$	200
17b	2	F	F	H	480
17c	2	F	F	CH_3	140
17d	2	F	F	CH_2CH_3	110
17e	2	F	F	$CH_2CH_2CH_3$	58
17f	2	F	F	$CH_2CH_2CH_2CH_3$	21
17g	2	F	F	$CH_2CH(CH_3)_2$	84
17h	2	F	F	$CH_2CH{=}CH_2$	9.8
17i	2	F	F	$CH_2C{\equiv}CH$	6.7
17j	2	F	F	$CH_2C{\equiv}CSi(CH_3)_3$	170
17m	2	F	F	$CH_2CH_2OCH_3$	120
19	3	F	F	$CH_2C{\equiv}CH$	72
Validation set	n	R^1	R^2	R^3	Ki(μM)
9i	2	H	H	$CH_2C{\equiv}CH$	7.8
8i	1	H	H	$CH_2C{\equiv}CH$	14
17k	2	F	F	$CH_2CO_2CH_2CH_3$	14
9d	2	H	H	CH_2CH_3	98
8f	1	H	H	$CH_2CH_2CH_2CH_3$	120
17l	2	F	F	CH_2CN	200
9b	2	H	H	H	210

2.2. Model Building

The structure of NtPPO (PDB ID: 1SEZ) [4] was downloaded (www.pdb.org) and prepared with Discovery Studio. Two monomers are present in the protein (A and B), we have used only A. No crystallographic water molecules were included in the model. The 3D structures of thecycloalka[d]quinazolinedione−benzoxazinones were constructed by Discovery Studio[10], on the basis of the crystal structure of 17a[4], and subsequently optimized with methods of algorithm *Smart Minimizer* before docking.

2.3. Molecular Mechanics

Modeling of ligands CQB and P-L complexes was carried out by molecular mechanics using CHARMm force field [11] as described earlier [12]

2.4. QSAR Model

Training set of 29 CQBs derivatives compounds with known inhibitory potencies towards the PPO [4], were docked to the binding site model of the PPO receptor model using the CDOCKER docking procedure [10]. Complexation QSAR models were elaborated for training set and a linear correlation was established between the computed Gibbs free energies of binding (GFE: $\Delta\Delta G_{com}$) and observed enzyme inhibition constants (K_i^{exp}) for each training set Were computed an QSAR models, which relate the K_i^{exp} to the computed scores, were prepared by linear regression analysis equation (1)

pK_i = f(Gibbs free energies) and *GFE = binding Energy of Complex($\Delta G_{binding}$) - Entropic Term ($T\Delta S$) + solvatation Energy (ΔG_{sol}) of Receptor*, which correlates the computed. The predictive power of Eq. (1), which was then used as the target-specific scoring function for the in silico screening of the designed virtual library CQB analogs, was verified by applying it to a validation set of 7 similar CQB inhibitors with known K_i^{exp} values, which were not included into the training set. The ratio of predicted activities K_i^{pre} obtained from the regression equation (1) and observed K_i^{exp} was used to evaluate the performance of the QSAR model.

2.5. Pharmacophore Generation

Bound conformations of inhibitors taken from the models of E-I complexes were used for constructing of 3D-QSAR pharmacophore (PH4) by using Catalyst HypoGen algorithm [13] implemented in Discovery Studio [10] as described earlier [14]

2.6. Virtual Library Generation

The virtual library generation was performed as described earlier [14]

2.7. Pharmacophore-Based Library searching

The pharmacophore model (PH4) described in Section 2.5 and derived from the bound conformations of CQBs at the active site of PPO served as a library searching tool as described earlier [14].

3. Results

3.1. Calculation of GFE and QSAR Model

The binding energy, *Entropic Term and solvation Energy* of the complex formation (*E:I*) , equation (1) [15], was computed for the 29 complexes from *docking* and the ratio of predicted and observed inhibition constants (pK_i^{pre}/pK_i^{exp}) for the validation set of 7 CQBs (not included into the training set) are listed, show in table 2. The QSAR model explained variation in the CQBs experimental potencies ($pK_i^{exp} = -\log_{10}(K_i^{exp})$ [xvi] by correlating it with computed GFE $\Delta\Delta G_{com}$ through linear regression (Equation (1) [12]. Table 2). In addition, significant correlation obtained in this QSAR relationship permitted to identify the CQBs active bound conformation at the PPO binding site and enabled definition of the PH4 pharmacophore. This correlation explained about 94% of the pK_i^{exp} data variation and underlined the role of the enthalpic contribution to the binding affinity of the ligand. Relatively high values of the regression coefficient R^2, the leave-one-out cross-validated regression coefficient R^2_{xv} and Fischer F-test of the correlation suggest strong relationship between the 3D model of ligand binding and the observed activation potencies of the CQBs

The statistical data of the regression are presented in Table 3.

Therefore, structural information derived from the 3D models of PPO:CQBx complexes can be expected to lead to reliable prediction of PPO activation potencies for new CQBs analogs based on the QSAR model.

Table2. *Gibbs free energy (binding affinity) and its components for the training set of PPO ligands CQBs and validation set ligands*

Training	Ki	$\Delta G_{binding}$	ΔG_{sol}	$T\Delta S$	ΔG_{compl}	$\Delta\Delta G_{compl}$	pKi

set	(µM)	(kcal/mol)	(kcal/mol)	(kcal/mol)	(kcal/mol)	(kcal)	
17i	0.0067	-58.79	-383.92	20.19	-462.90	0.00	8.17
17h	0.0098	-56.99	-383.42	20.20	-460.62	2.28	8.01
9h	0.011	-57.56	-382.94	19.98	-460.48	2.42	7.96
8h	0.02	-55.37	-383.61	20.36	-459.33	3.56	7.7
17f	0.021	-55.27	-382.60	20.36	-458.22	4.67	7.68
9k	0.037	-55.26	-382.90	20.24	-458.40	4.50	7.43
9e	0.044	-54.29	-382.90	20.02	-457.21	5.69	7.36
9f	0.046	-54.90	-382.56	20.15	-457.61	5.29	7.34
8k	0.048	-54.36	-382.26	20.14	-456.77	6.13	7.32
17e	0.058	-53.09	-382.99	20.22	-456.30	6.60	7.24
8e	0.069	-52.32	-383.16	19.91	-455.39	7.51	7.16
19	0.072	-53.94	-382.85	20.36	-457.15	5.75	7.14
17g	0.084	-52.66	-382.61	20.30	-455.57	7.33	7.08
8d	0.098	-51.19	-382.61	19.78	-453.57	9.33	7.01
9g	0.1	-51.88	-382.83	20.10	-454.81	8.09	7
9l	0.11	-51.06	-383.04	19.99	-454.09	8.81	6.96
17d	0.11	-51.17	-382.89	20.12	-454.18	8.72	6.96
17m	0.12	-51.00	-383.88	20.36	-455.24	7.65	6.92
17c	0.14	-51.45	-383.55	20.04	-455.03	7.86	6.85
9c	0.16	-49.96	-383.33	19.80	-453.10	9.80	6.8
17j	0.17	-49.69	-382.60	20.01	-452.30	10.60	6.77
8g	0.17	-51.97	-381.34	20.01	-453.32	9.57	6.77
9a	0.2	-51.07	-382.35	20.51	-453.93	8.97	6.7
17a	0.2	-50.55	-382.12	20.69	-453.35	9.55	6.7
8a	0.21	-51.18	-382.11	20.41	-453.69	9.21	6.68
9j	0.26	-49.73	-381.67	20.50	-451.90	11.00	6.59
8c	0.27	-49.35	-383.32	19.68	-452.36	10.54	6.57
8b	0.34	-49.04	-383.76	19.57	-452.37	10.52	6.47
17b	0.48	-47.26	-384.00	19.94	-451.20	11.70	6.32
8j	2.5	-45.55	-384.04	19.10	-448.69	14.21	5.60
Validation set	**Ki**	**ΔGbinding (kcal/mol)**	**ΔGsol (kcal/mol)**	**TΔS (kcal/mol)**	**ΔGcompl (kcal/mol)**	**pKi_théo**	**pki_théo/pki_exp**
9i	0.0078	-56.88	-383.52	19.97	-460.38	7.91	0.974
8i	0.014	-57.57	-383.00	19.86	-460.44	7.92	1.009
17k	0.014	-57.87	-382.75	20.54	-461.16	8.05	1.025
9d	0.098	-52.90	-382.98	19.90	-455.78	7.13	1.017
8f	0.12	-52.27	-382.93	20.01	-455.21	7.03	1.016
17l	0.2	-50.02	-383.01	20.22	-453.26	6.70	1.000
9b	0.21	-49.94	-383.79	19.71	-453.44	6.73	1.008

Table 3. Analysis of computed binding affinities ΔΔGcom and experimental activity effective concentration of CQBs towards PPO [14]

Statistical Data of Linear Regression	
pK_i^{exp} = -0.1664 $\Delta\Delta G_{com}$ + 8.306	(1)
Number of compound n	29
Squared correlation coefficient of regression R^2	0.94
LOO cross-validated squared correlation coef R^2_{xv}	0.94
Standard error of regression σ	0.132
Statistical significance of regression, Fisher F-test	449.36
Level of statistical significance α	>95%
Range of activities K_i^{exp} [nM]	6.7-2500

The statistical data confirmed validity of the correlation Equations (1) plotted on Figure 3.The ratio pK_i^{pre}/pK_i^{exp} (the pK_i^{pre} values were estimated using correlation Equation (1), Table 3) calculated for the validation set documents the substantial predictive power of the complexation QSAR model from Table 2. Thus, the regression Equation (1) (Table 3) and computed $\Delta\Delta G_{com}$ GFEs can be used for prediction of activator potencies K_i^{pre} against PPO for novel CQB analogs, provided they share the same binding mode as the training set.

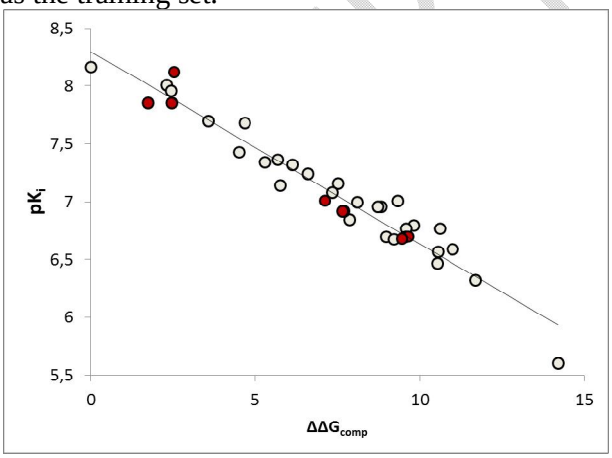

Figure 3. Plot for relative complexation Gibbs free energies of the PPO-CQBx complex formation $\Delta\Delta G_{com}$ [kcal.mol^{-1}] of the training set [xvi]. The validation set data points are shown in red color.

3.2. QSAR Pharmacophore Model

PPO activation 3D-QSAR pharmacophore was generated from the active conformation of 29 TS CQBx and evaluated by 7 VS CQB covering a large range of experimental activity (6.7–2500 nM) spanning more than

two orders of magnitude. The generation process is divided into three main steps: (i) the constructive step, (ii) the subtractive step and (iii) the optimization step [10]

During the constructive phase. 17i alone was retained as the lead (since only the activity of 17i fulfilled the threshold criterion. $K_i^{exp} \leq 1.2 \times 8$ nM) and used to generate the starting PH4 features. In the subtractive phase, compounds for which $K_i^{exp} > 8 \times 103.5$ nM = 25.298 nM were conside-red inactive. Accordingly none of the training set CQBx was inactive and no starting PH4 features were removed. Finally, during the optimization phase, the score of the pharmacophoric hypotheses was improved. Hypotheses were scored according to errors in activity estimates from regression and complexity via a simulated annealing approach. At the end of the optimization, the top scoring 10 unique pharmacophore hypotheses were kept, all displaying five-point features. The cost values, correlation coefficients, root-mean square deviation (RMSD) values, the pharmacophore features, and the max-fit value of the top 10 ranked hypotheses (Hypo1- Hypo10) are listed in Table 4.

Table 4. Parameters of 10 generated PH4 pharmacophoric hypotheses for PPO ligand after Cat-Scramble validation procedure (49 scrambled runs for each hypothesis at the selected level of confidence of 98%).

Hypothesis[a]	RMSD[b]	R^2	Total costs[c]	Costs Difference[d]
Hypo 1	5.35	0.91	475.78	1994.95
Hypo 2	5.52	0.90	503.08	1967.65
Hypo 3	5.68	0.89	529.64	1941.09
Hypo 4	5.76	0.89	544.18	1926.55
Hypo 5	5.79	0.89	549.03	1921.70
Hypo 6	5.79	0.89	549.23	1921.50
Hypo 7	5.81	0.89	551.80	1918.92
Hypo 8	5.86	0.88	559.82	1910.91
Hypo 9	5.87	0.88	562.11	1908.62
Hypo 10	6.08	0.87	597.58	1873.15

[a]root mean square deviation; [b] squared correlation coefficient; [c] overall cost parameter of the PH4 pharmacophore; [d] cost difference between Null cost and hypothesis total cost; [e] lowest cost from 49 scrambled runs at a selected level of confidence of 98%. The Fixed Cost = 43.48 with RMSD = 0, the Null Cost = 2470.73 with RMSD = 12.76 and the Configuration cost = 14.78.

The generated pharmacophore models were then assessed for their reliability based on the calculated cost parameters ranging from 475.78 (Hypo1) to 597.58 (Hypo10). The relatively small gap between the highest and lowest cost parameter corresponds well with the homogeneity of the generated hypotheses and consistency of the TS of CQBx. For this PH4 model, the fixed cost (43.48) is lower than the null cost (2470.73) by a difference Δ = 2427.25. This difference is a major quality indicator of the PH4 predictability ($\Delta > 70$ corresponds to an excellent chance or a probability higher than 90% that the model represents a true correlation [10]. To be statistically significant, a hypothesis has to be as close as possible to the fixed cost and as far as possible from the null cost. For the set of 10 hypotheses, the difference $\Delta \geq$ 597.58 which attests to the high quality of the pharmacophore model. The standard indicators such as the RMSD between the hypotheses ranged from 5.35 to 6.08, and the squared correlation coefficient (R^2) falls to an interval from 0.91 to 0.87. The first PH4 hypothesis with the total costs (475.78) and best RMSD and R^2 was retained for further analysis. The statistical data for the set of hypotheses (costs, RMSD, R^2) are listed in Table 4. The configuration cost (14.78 for all hypotheses) below 17 confirms this pharmacophore as a reasonable one. The evaluation of Hypo 1 is the mapping of the best active training set 17i (Figure 4 (D)) displaying the geometry of the Hypo1 pharmacophore of PPO activation. The regression equation for pK_i^{exp} vs. pK_i^{pre} estimated from Hypo1: $pK_i^{exp} = 0.947 \times pKi_{pre} + 0.41(2)$ (n = 29. $R^2 = 0.91$. $R^2_{xv} = 0.91$. F-test = 292.32. $\sigma = 0.16$, $\alpha > 95$ %) is also plotted on Figure 4 (E). The ratio pK_i^{pre}/pK_i^{exp} (the pK_i^{pre} values were estimated using correlation Equation ((2), Table 5) calculated for the training set and validation set is near of the 1. Therefore the PH4 is good potentially to choice the new CQB analogs.

We can carry out computational design and selection of new CQB analogs with elevated activation potencies against PPO.

Table 5: The ratio pK_i^{pre}/pK_i^{exp} calculated for the training set and validation set

Training set	pK_i^{pre}	pK_i^{exp}	pK_i^{pre}/pK_i^{exp}
17i	8.02	8.17	0.981
17h	7.84	8.01	0.979
9h	7.77	7.96	0.976
17f	7.76	7.68	1.011
8h	7.74	7.7	1.006
9f	7.74	7.34	1.055
9e	7.35	7.36	0.999
17e	7.33	7.24	1.013
19	7.27	7.14	1.019
9k	7.27	7.43	0.978
8k	7.19	7.32	0.982
8e	7.18	7.16	1.003
9g	7.05	7	1.006
17g	7.02	7.08	0.992
17d	6.97	6.96	1.001
8d	6.84	7.01	0.975
8g	6.75	6.77	0.997
9l	6.71	6.96	0.965
17a	6.70	6.7	1.001
9a	6.70	6.7	1.000
9j	6.69	6.59	1.015
17c	6.68	6.85	0.975
17j	6.68	6.77	0.986
17b	6.67	6.32	1.056
17m	6.65	6.92	0.961
9c	6.55	6.8	0.964
8a	6.51	6.68	0.974
8b	6.40	6.47	0.990
8c	6.35	6.57	0.966
8j	5.60	5.6	1.001
Validation set	**pKi_theo**	**pKi_exp**	**pKi_theo/pki_exp**
9i	8.10	8.12	0.998
8i	7.85	7.85	1.000
17k	7.85	7.85	1.000
9d	7.05	7.01	1.006
8f	6.97	6.92	1.007
17l	6.76	6.7	1.009
9b	6.74	6.68	1.009

3.3. Virtual Screening

In silico screening of a virtual (combinatorial) library can lead to hit identification as it was shown in our previous works on inhibitors design [15,xvii,xviii,xix,xx,xxi]. An initial virtual library (VL) was generated by substitutions at positions for R_1, R_2 and R_3 (Table 5) on the CQB scaffold. During the virtual library

enumeration the R-groups listed in Table 5 were attached to in positions R_1.R_2 and R_3 of the CQB scaffold to form a combinatorial library of the size:

$R_1 \times R_2 \times R_3 = 1 \times 1 \times 118 = 118$ analogs.

The focused library of 118 analogs was further screened for molecular structures matching the 3D-QSAR PH4 pharmacophore model Hypo1 of PPO activation, 28 best fitting analogs (PH4 hits) then underwent complexation QSAR model screening. The computed GFE of PPO-CQBx complex formation, their components and predicted activity Ki_{pre} calculated from the correlation Equation (1) (Table 3) are listed in Table 6.

3.4. Novel CQB Analogs

The design of virtual library of novel analogs was guided by structural information retrieved from the CQBx active conformation and the pharmacophore model, were used for the selection of appropriate substituents. The hydrophobic feature of PH4 at the position R_3 show clearly the type of group.

4. Discussion

4.1. Binding mode Cycloalka[d]quinazoline-2,4dione−Benzoxazinones

In more the good quality of the QSAR model, pharmacophore and the focusing catalytic pocket of PPO interactions between the CQB and active site residues such as Leu334, Phe392, Leu372, and Leu356 are revealing. The key interactions responsible for the CQB affinity to PPO, such as hydrogen bonds, van der Waals interactions, and hydrophobic contacts, etc. As displayed in the 2D of Figure 2, the binding of 17i most active ligand in the TS to the active site of PPO is supported by this interactions. This analysis indicates that compounds with hydrophobic groups may be advantageous to PPO-inhibiting activity.

4.2. Analysis of new ligands from in silico screening

An analysis of structural requirement for PPO activation at the level of hydrophobic contacts with the active site revealed that the substituent at R_3 table6. In this job, the use of the pharmacophore model new method to select the best analogs. The theoretical activities calculated by equation (1) are show in table7. Top scoring virtual hits analogs of CQB are: CQB1 (0,75nM), CQB11 (0,71nM) and CQB22 (0,29nM). The predicted activity of the best designed CQB analog CQB22 (figure 5) reached approximately 23 times lower than that of the most active ligand of the training set 17i with K_i^{exp} = 6.7 nM (Table 8).

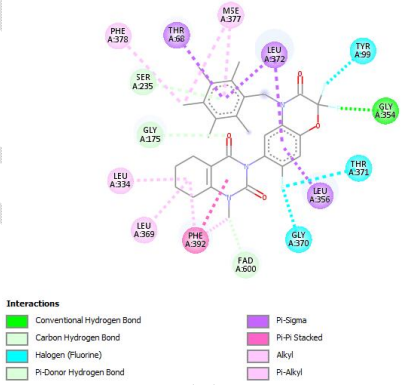

(A)

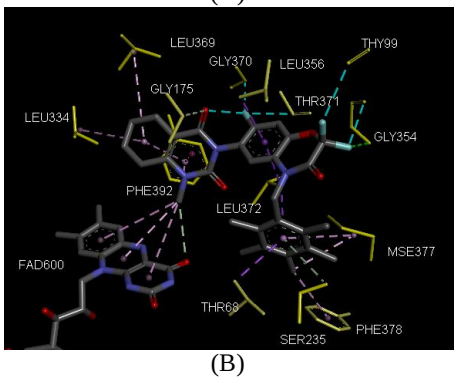

(B)

Figure 5 : (A) 2D schematic interaction diagram of the most potent inhibitor CQB22 at the active site of PPO and (B) 3D schematic interaction.

5. conclusion

Structural investigation of the SAR of Cycloalka[d]quinazoline-2,4dione-Benzoxazinones as partial PPO agonists from the crystal structure of PPO: CQB complex guided us during preparation of a reliable QSAR model of activation of PPO which correlated computed Gibbs free energies upon complex formation with observed PPO activation potencies. In addition we have derived a 3D-QSAR PH4 pharmacophore model for CQB activation using a training set of 29 and validation set of 7 CQBs with known activation activities [8]. Careful analysis of interactions between the FXR's active site residues and AADs directed us in the design of an initial diversity virtual combinatorial library of new CQB analogs with multiple substitutions hydrophobic group in R_3. A library screened by matching of the analogs to the PH4 pharmacophore permitted selection of a library subset of CQBs. This subset of 28 best virtual hits was submitted to computation of predicted activation potencies by the complexation QSAR model. The hit analogs reached predicted activities in the nanomolar concentration range. The hit designed CQB analogs are CQB1 (0.75 nM), CQB11 (0.71 nM) and CQB22 (0.29 nM)) are recommended for synthesis and subsequent activity evaluation in PPO activation assays and may lead to a discovery of novel weedkiller potent partial PPO agonists. Virtual design method is an excellent trail already use in medicinal chemistry for discovery a good diseases targets therefore the researchers must apply it more in agropastoral.

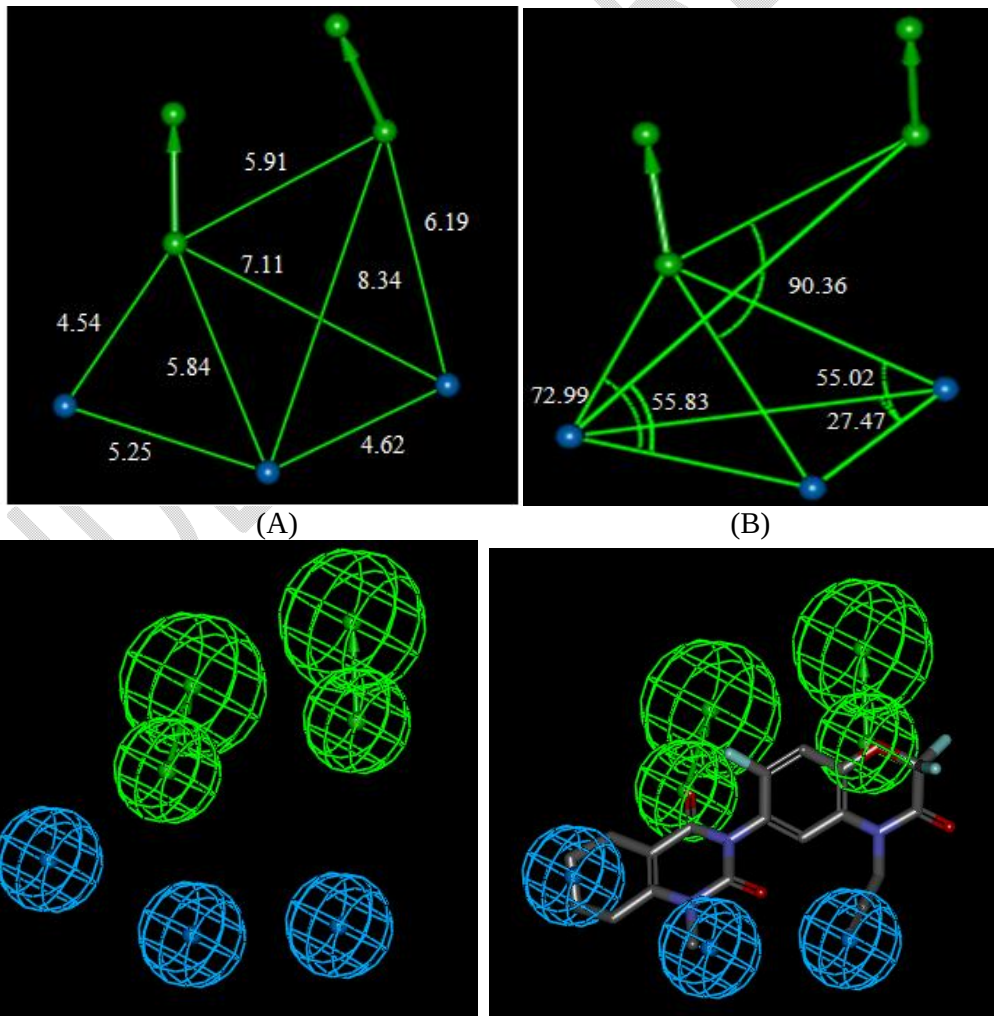

(A) (B)

(B) (D)

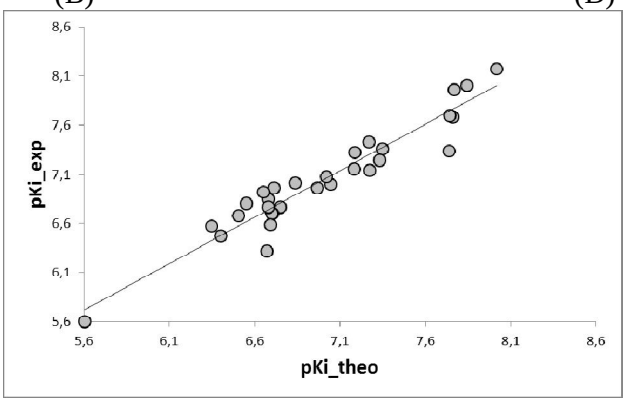

(E)

Figure 4. (A) Distances between centers, (B) angles between centers of pharmacophoric features (C) features, (D) mapping of pharmacophore of ligand with the most partial agonist 17i. Feature legend: HYDA = Hydrophobic Aliphatic (blue), HBA = Hydrogen bond Acceptor (green). (E) Correlation plot of experimental vs. predicted activation activity

Table 6. R-groups (fragments. building blocks. substituents) used in the design of the diversity VL of CQB analogs.

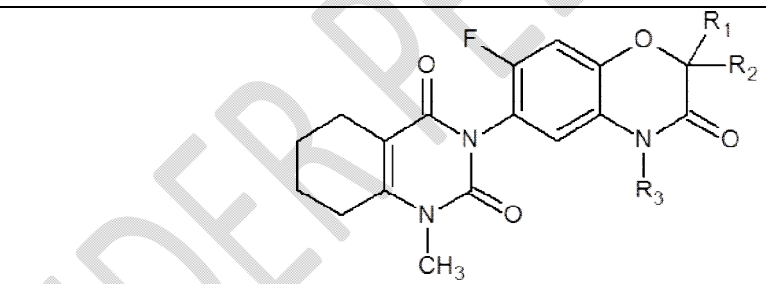

R_1=R_2=Fluor (F)					
R_3					
1	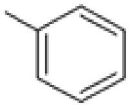	11	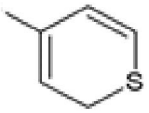	21	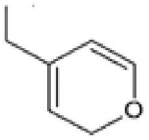
2	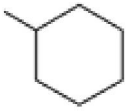	12	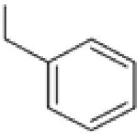	22	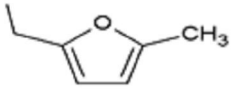

3	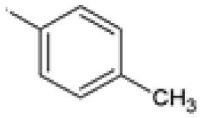	13	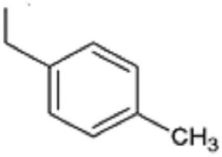	23	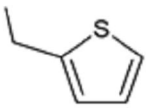
4	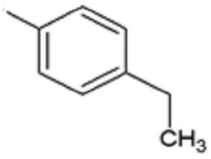	14	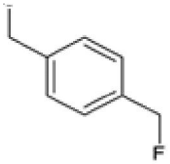	24	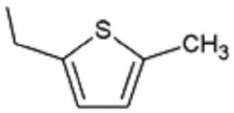
5	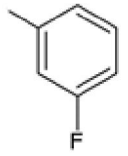	15	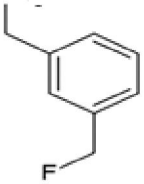	25	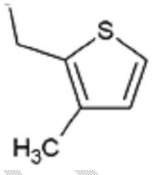
6	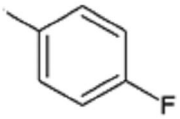	16	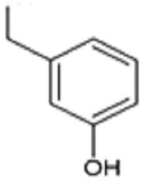	26	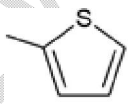
7	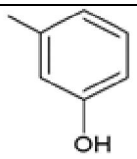	17	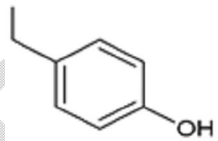	27	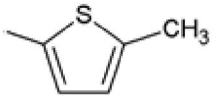
8	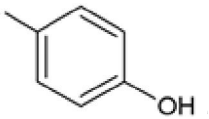	18	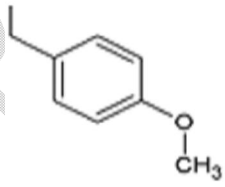	28	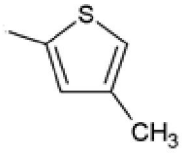
9	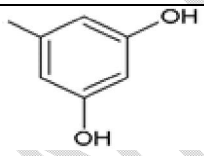	19	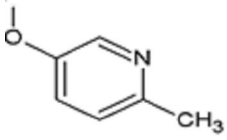	29	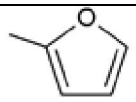
10	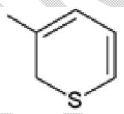	20	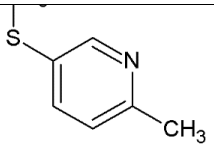	30	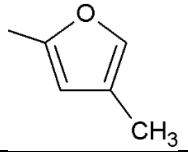
N°	R	N°	R	N°	R
31	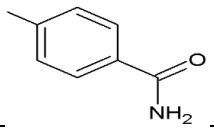	41	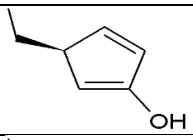	51	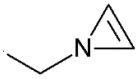
32	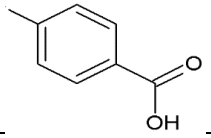	42	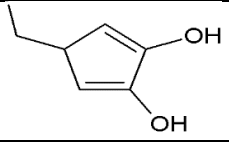	52	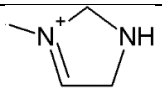

33	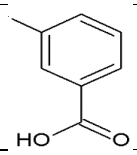	43	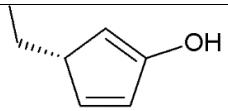	53	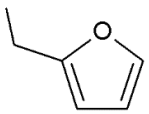
34	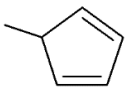	44	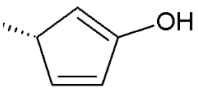	54	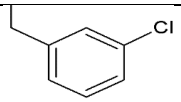
35	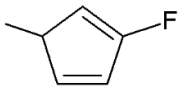	45	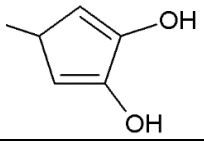	55	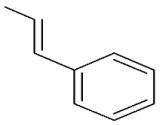
36	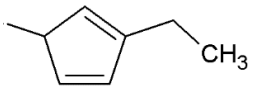	46	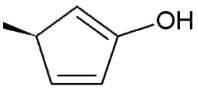	56	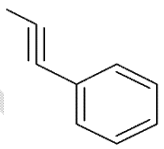
37	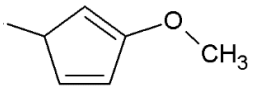	47		57	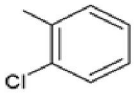
38	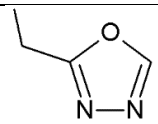	48		58	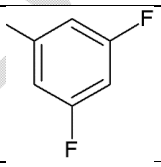
39	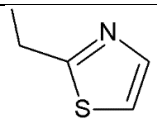	49	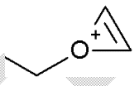	59	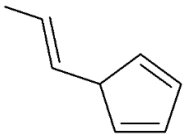
40	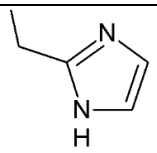	50	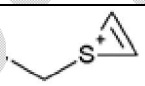	60	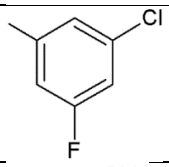
61	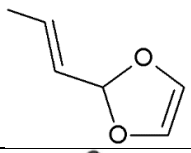	71	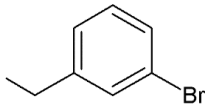	81	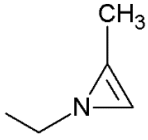
62	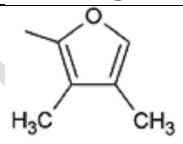	72	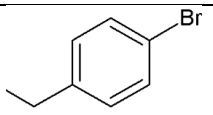	82	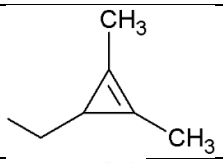
63	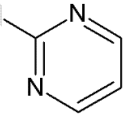	73	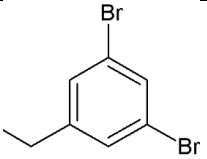	83	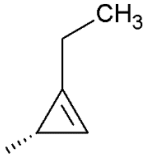

64	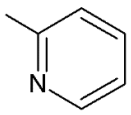	74	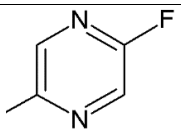	84	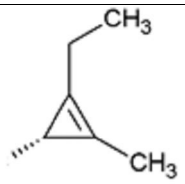
65	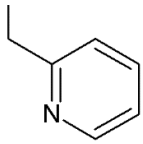	75	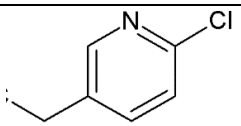	85	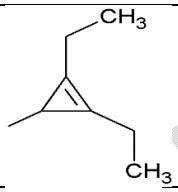
66	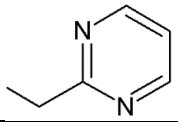	76	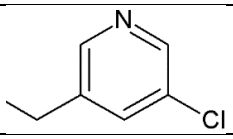	86	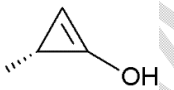
67	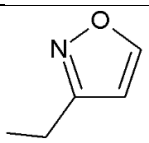	77	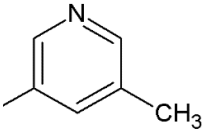	87	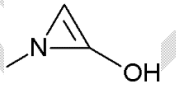
68	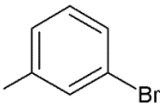	78	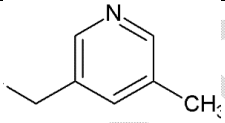	88	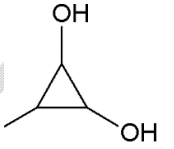
69	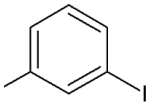	79	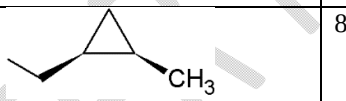	89	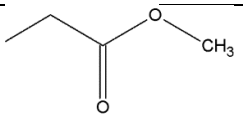
70	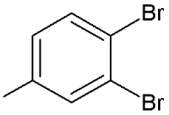	80	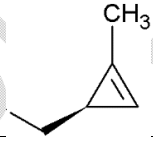	90	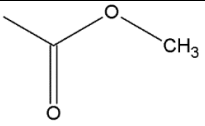
91	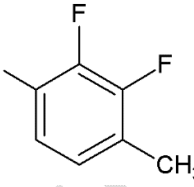	92	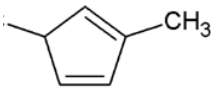	92	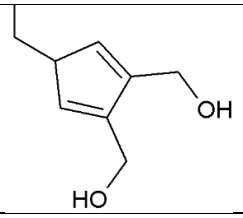
93	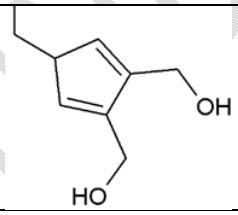	94	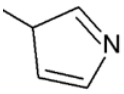	95	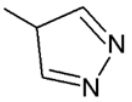
96	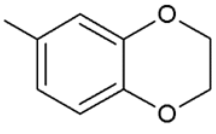	97	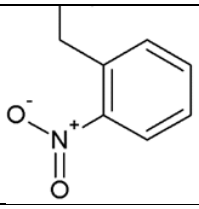	98	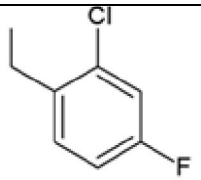

99	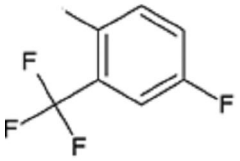	100	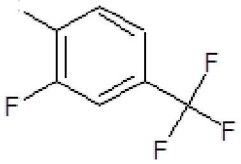	101	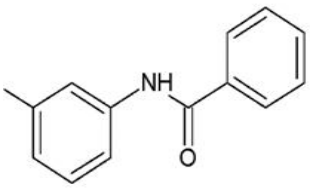
102	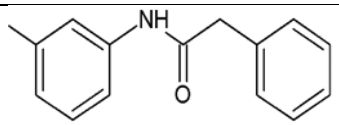	103	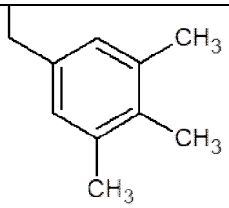	104	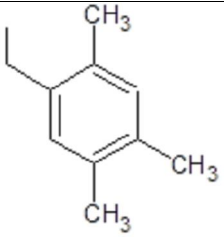
105	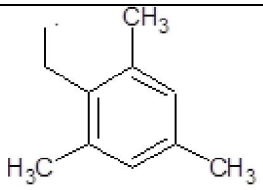	106	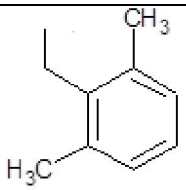	107	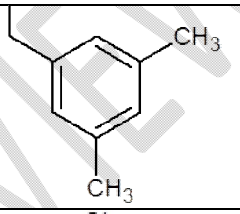
108	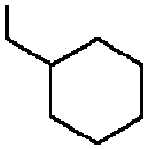	109	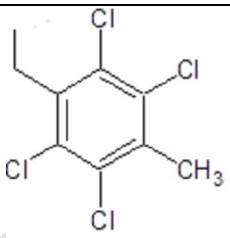	110	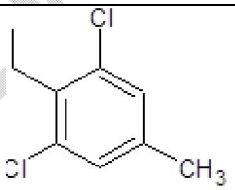
111	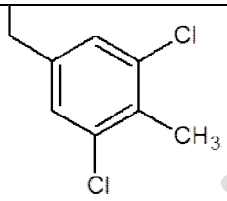	112	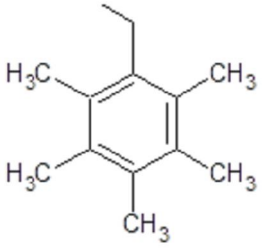	113	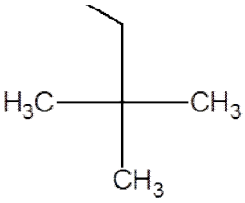
114	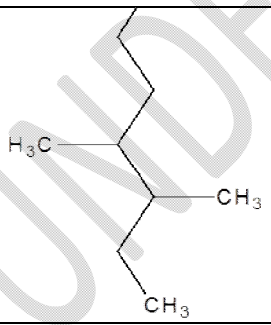	115	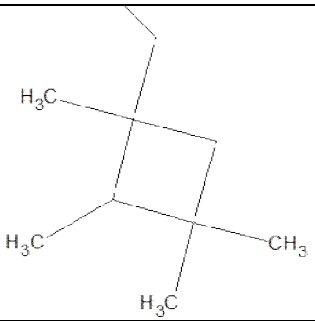	116	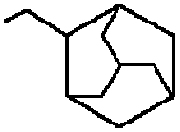
117	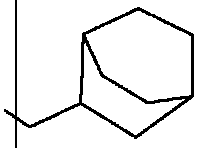	118	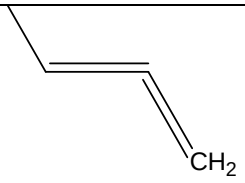		

Table7 : CQB analogues inhibitors of PPO

Analogues	ΔGbinding	ΔGsol (kcal)	TΔS (kcal)	ΔGcompl (kcal)	ΔΔGcompl (kcal)	Ki_theo(nM)
17i	-58.79	-383.92	20.19	-462.90	0.00	6.7
CQB1	-61.43	-385.56	20.81	-467.80	-4.90	0.76
CQB2	-56.15	-383.95	20.58	-460.67	2.22	11.6
CQB3	-51.25	-383.64	20.52	-455.41	7.49	87.1
CQB4	-51.25	-384.16	20.29	-455.70	7.20	78.4
CQB5	-54.24	-384.04	20.41	-458.69	4.21	24.8
CQB6	-56.74	-384.02	20.41	-461.17	1.73	9.6
CQB7	-53.13	-384.35	20.33	-457.81	5.09	34.7
CQB8	-51.26	-383.74	20.57	-455.58	7.32	81.7
CQB9	-51.35	-383.70	20.61	-455.66	7.24	79.1
CQB10	-49.48	-384.05	20.51	-454.04	8.86	147.4
CQB11	-63,28	-383.44	21.24	-467.96	-5.06	0.7
CQB12	-62.47	-382.09	20.76	-465.32	-2.43	1.9
CQB13	-62.64	-380.04	20.80	-463.48	-0.59	3.9
CQB14	-57.81	-385.56	20.81	-464.18	-1.28	3.03
CQB15	-60.46	-383.37	20.68	-464.52	-1.62	2.7
CQB16	-61.44	-380.12	20.65	-462.21	0.68	6.4
CQB17	-63.13	-378.77	21.24	-463.14	-0.25	4.5
CQB18	-60.61	-380.06	21.27	-461.94	0,95	7.1
CQB19	-60.06	-383.50	20.98	-464.55	-1.65	2.6
CQB20	-55.99	-383.80	20.81	-460.60	2.30	11.9
CQB21	-53.72	-384.39	20.82	-458.92	3.97	22.7
CQB22	-69.39	-380.01	20.86	-470.26	-7.36	0.29
CQB23	-54.31	-379.73	20.39	-454.42	8.48	127.2
CQB24	-58.82	-379.58	20.71	-459.10	3.79	21.1
CQB25	-61.84	-379.71	20.65	-462.20	0.70	6.5
CQB26	-61.78	-379.78	20.81	-462.37	0.52	6.04
CQB27	-58.60	-380.12	20.67	-459.39	3.51	18.9
CQB28	-50.35	-380.47	20.26	-451.08	11.82	458.5

Table 8 : CQB analogues inhibitors of PPO, depicted in 2D,

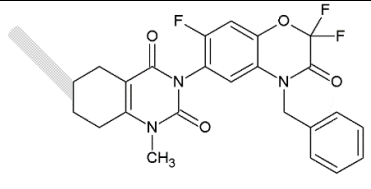	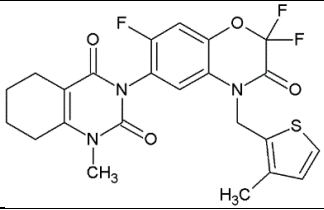	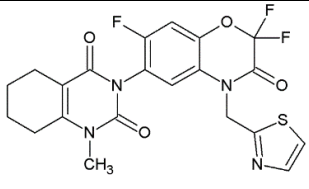
CQB1 (0,75nM)	CQB2(11,6nM)	CQB 3(87 ,09nM)
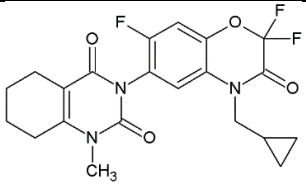	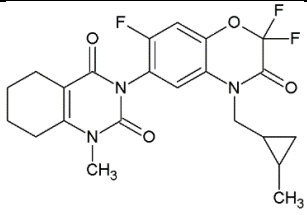	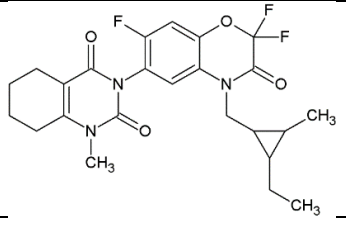

CQB 4(78,04nM)	CQB 5(24,8nM)	CQB6(9,6nM)
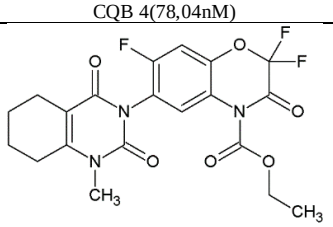	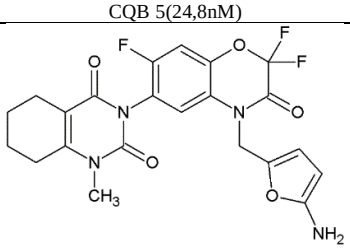	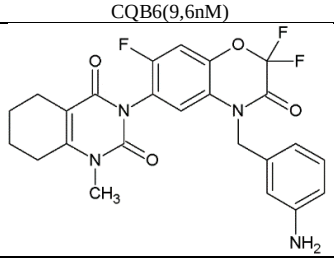
CQB7(34,7nM)	CQB 8(81,7nM)	CQB 9(79,06nM)
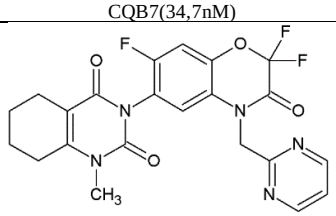	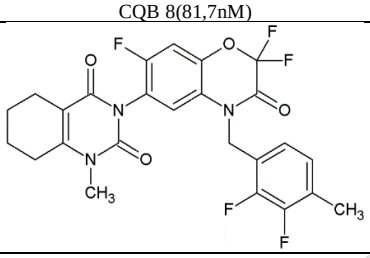	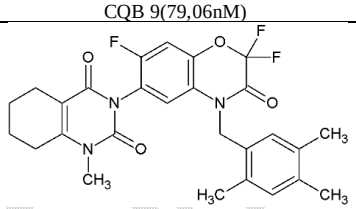
CQB 10(147,4nM)	CQB 11(0,71nM)	CQB12 (1,95nM)
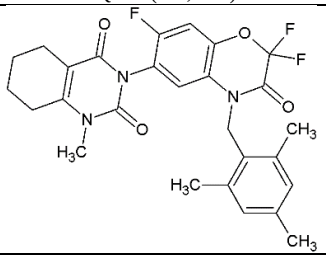	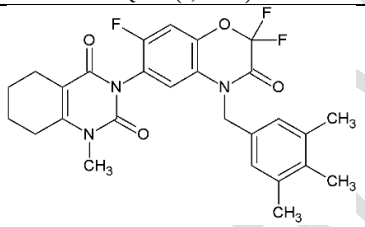	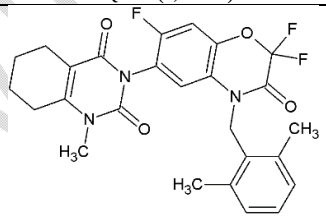
CQB13 (3.9nM)	CQB14 (3,03nM)	CQB15 (2,7nM)
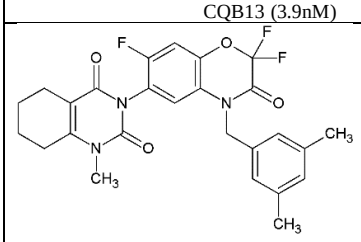	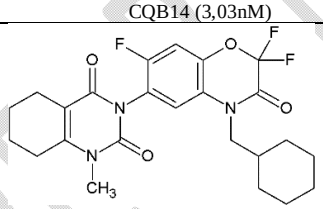	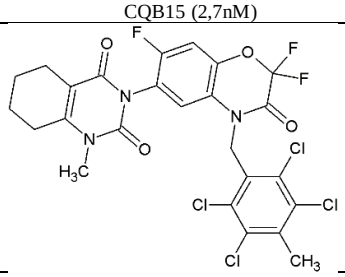
CQB16:1(7,2nM)	CQB17 (4,5nM)	CQB18 (:7,1nM)
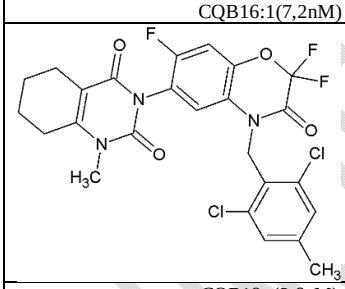	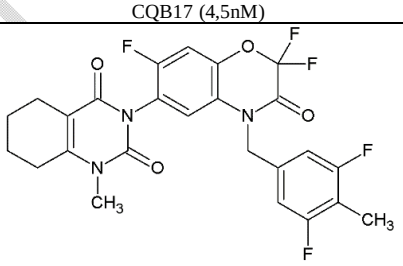	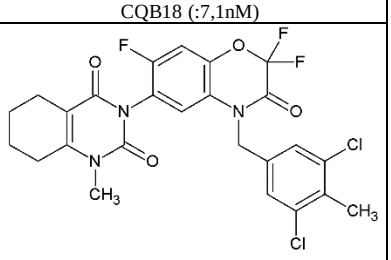
CQB19 :(2,6nM)	CQB20 :(11,,9nM)	CQB21 :(5,2nM)
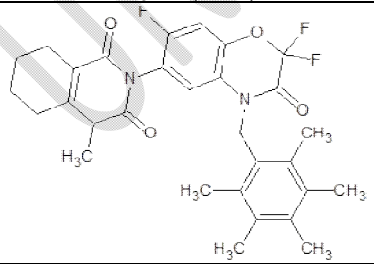	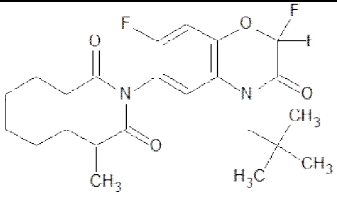	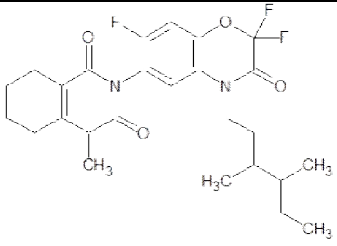
CQB22 :(0,29nM)	CQB23 :(127,14nM)	CQB24 :(21,1nM)

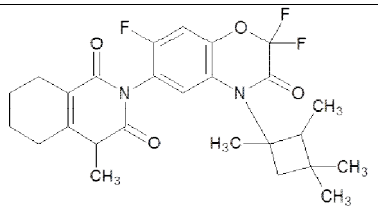	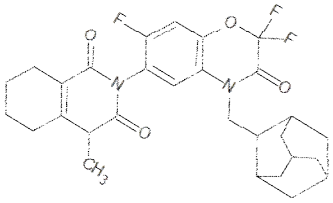	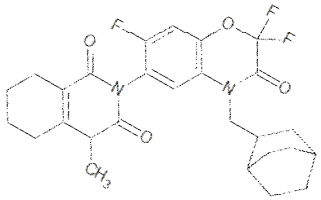
CQB25 :(6,45nM)	CQB26 : (6,04nM)	CQB27 : (18,9nM)
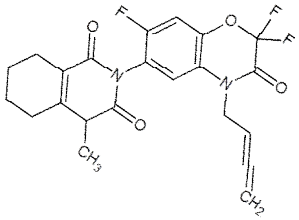		
CQB28:(458,5nM)		

REFERENCES

[1] https://www.un.org/sustainabledevelopment/sustainable-development-goals/

[2] Wang, B.; Wen, X.; Xi, Z. Molecular simulations bring new insights into protoporphyrinogenIX oxidase / protoporphyrinogen IX interaction modes. Mol. Inf. 2016, 35, 476−482

[3] Hao, G. F.; Tan, Y.; Xu, W. F.; Cao, R. J.; Xi, Z.; Yang, G. F. Understanding resistance mechanism of protoporphyrinogen oxidase inhibiting herbicides: insights from computational mutation scanning and site-directed mutagenesis. J. Agric. Food Chem. 2014, 62, 7209− 7215

[4] Da-Wei Wang, Rui-Bo, Shu-Yi Yu, Lu Liang, Imail Ismail, Yang-Hong Li, Han Xu, Xin Wen, Zhen Xi. Design, herbicidal Activity, and QSAR Analysis of cycloalka[d]quinazoline-2,4-dione-BenzoxazinoneS as Protoporphyrinogen IX oxidase. Journal of Agricultural and Food chemistry 2019, 67 (33), 9254-9264.

[5] Zuo, Y.; Wu, Q.; Su, S. W.; Niu, C. W.; Xi, Z.; Yang, G. F. Synthesis, herbicidal activity, and QSAR of novel N-benzothiazolyl pyrimidine-2,4-diones as protoporphyrinogen oxidase inhibitors. J. Agric. Food Chem. 2016, 64, 552−562.

[6] Wang, D. W.; Li, Q.; Wen, K.; Ismail, I.; Liu, D. D.; Niu, C. W.; Wen, X.; Yang, G. F.; Xi, Z. Synthesis and herbicidal activity of pyrido[2,3-d]pyrimidine-2,4-dione-benzoxazinone hybrids as proto porphyrinogen oxidase inhibitors. J. Agric. Food Chem. 2017, 65, 5278−5286. (24)

[7] Jiang, L.-L.; Tan, Y.; Zhu, X.-L.; Wang, Z.-F.; Zuo, Y.; Chen, Q.; Xi, Z.; Yang, G.-F. Design, synthesis, and 3D-QSAR analysis of novel 1,3,4-oxadiazol-2(3H)-ones as protoporphyrinogen oxidase inhibitors. J. Agric. Food Chem. 2010, 58, 2643−2651.

[8] Design, Synthesis, and Herbicidal Activity of Novel Diphenyl Ether Derivatives Containing Fast Degrading Tetrahydrophthalimide
Li-Xia Zhao, Mao-Jun Jiang, Jia-Jun Hu, Yue-Li Zou, Yuan Cheng, Tao Ren, Shuang Gao, Ying Fu,*and Fei YeJ. Agric. Food Chem. 2020, 68, 3729−3741

[9] Li, H.; Sutter, J.; Hoffmann, R. Pharmacophore Perception, Development and Use in Drug Design; Güner, O.F., Ed.; International University Line: La Jolla, CA, USA, 2000; pp. 171-189.

[10] Discovery Studio Molecular Modeling and Simulation Program, version 2.5; Accelrys, Inc.: San Diego, CA, USA, 2009. (n.d.)

[11] Maple JR, Hwang M-J, Stockfisch TP, et al. Derivation of class II force fields. I. Methodology and quantum force field for the alkyl functional group and alkane molecules. J. Comput. Chem. 1994; 15(2): 162- 182. View Article

[12] Kouassi A, Kone M, Keita M, et al. Computer-Aided Design of Orally Bioavailable Pyrrolidine Carboxamide Inhibitors of Enoyl-Acyl Carrier Protein Reductase of Mycobacterium tuberculosis with Favorable Pharmacokinetic Profiles. Int. J. Mol. Sci. 2015; 16(12): 29744-29771. PMid:26703572 View Article PubMed/NCBI

[13] Li, H.; Sutter, J.; Hoffmann, R. Pharmacophore Perception, Development and Use in Drug Design; Güner, O.F., Ed.; International University Line: La Jolla, CA, USA, 2000; pp. 171-189.

[14] Kouassi, A.F.; Kone, M.; Keita, M.; Esmel, A.; Megnassan, E.; N'Guessan, Y.T.; Frecer, V.; Miertus, S. Computer-aided design of orally bioavailable pyrrolidine carboxamide inhibitors of Enoyl-Acyl Carrier Protein Reductase of Mycobacterium tuberculosis with favorable pharmacokinetic profiles. Int. J. Mol. Sci. 2015, 16, 29744-29771. PMid:26703572 View Article PubMed/NCB

[15] Kouman KC, Keita M, Kre N'Guessan R, et al. Structure-Based Design and in Silico Screening of Virtual Combinatorial Library of Benzamides Inhibiting 2- trans Enoyl-Acyl Carrier Protein Reductase of Mycobacterium tuberculosis with Favorable Predicted Pharmacokinetic Profiles. Int. J. Mol. Sci. 2019; 20(19): 4730. PMid:31554227 View Article PubMed/NCBI

[xvi] Merk D, Lamers C, Ahmad K, et al. Extending the Structure-Activity Relationship of Anthranilic Acid Derivatives As Farnesoid X Receptor Modulators: Development of a Highly Potent Partial Farnesoid X Receptor Agonist. J. Med. Chem. 2014; 57(19): 8035- 8055. PMid:25255039 View Article PubMed/NCBI

[xvii] N'Guessan H, Megnassan E. Design of Phosphonic Arginine and Hydroxamic Acid Inhibitors of Plasmodium falciparum M17 Leucyl Aminopeptidase with Favorable Pharmacokinetic Profile. J. Drug Des. Med. Chem. 2017; 3(6): 98. View Article

[xviii] Allangba KNPG, Keita M, Kre N'Guessan R, Megnassan E, Frecer V, Miertus S. Virtual design of novel Plasmodium falciparum cysteine protease falcipain-2 hybrid lactone-chalcone and isatin-chalcone inhibitors

probing the S2 active site pocket. J. Enzyme Inhib. Med. Chem. 2019; 34(1): 547-561. PMid:30696325 View Article PubMed/NCBI

[xix] Esmel, A.; Keita, M.; Megnassan, E.; Beguemsi, T.; Frecer, V.; Miertus, S. Insight into the binding mode of nitrile inhibitors of Plasmodium falciparum falcipain-3, QSAR and pharmacophore models, virtual design of new analogs with favorable pharmacokinetic profiles. SDRP J. Comput. Chem. Mol. Model. 2018, 2, 103-124. View Article

[xx] Guy Guy Müller Banquet OKRA, Raymond Kre N'Guessan, Dali Brice, Hermann N'Guessan, Affiba Florance Kouassi, Conformational analysis and molecular design of anthranilic acid derivatives as partial agonists of the Farnesoid X Receptor (FXR) with favorable predicted pharmacokinetic profiles SDRP J. Comput. Chem. Mol. Model (2021) 5(2) p:585-605 View Article

[xxi] Yéo Yaya ,Melalie Keita, , Bibila Mayaya Bisseyou Yvon , Akori Elvice Esmel, Brice Dali, Hermann N'Guessan, Molecular and Thermodynamic Modeling of the Protein-Ligand Interaction. Application to Computer-Assisted Design of Anti-Competitive Inhibitors of Human Histone Deacetylase 2 (HDAC2). SDRP J. Comput. Chem. Mol. Model (2021) 5(2) p:585-609